

# Nuclear spin-independent and dependent parity non-conservation in $^{171}\text{Yb}^+$ using perturbed relativistic coupled-cluster theory

B. K. Mani

*Department of Physics, University of South Florida, Tampa, Florida 33620, USA*

We present nuclear spin-independent and dependent parity non-conservation amplitudes for the  $[4f^{14}]6s^2S_{1/2} - [4f^{14}]5d^2D_{3/2}$  transition of  $^{171}\text{Yb}^+$ , calculated using perturbed relativistic coupled-cluster theory. As a proxy to estimate theoretical uncertainty of these results we calculate the excitation energies, hyperfine structure constants and E1 transition amplitudes for the important low lying states. The PNC results presented in paper shall be useful in the propose PNC experiments.

PACS numbers: 31.15.bw, 11.30.Er, 31.15.am

## I. INTRODUCTION

The theoretical results of atomic parity non-conservation (PNC) when combined with the experimental results is an important probe of physics beyond the standard model of particle physics [1]. There are two sources of PNC in atoms, nuclear spin-independent (NSI) and nuclear spin-dependent (NSD). The NSI-PNC is well studied and experimentally observed in several atoms. The most precise measurement till date is in the case of atomic Cs [2]. The same experiment also indicated a signature of NSD-PNC effects. The most dominant source of which is the nuclear anapole moment (NAM), a parity violating interaction within the nucleus [3–5]. However, there are two other contributions to NSD-PNC, these are the NSD electron-nucleus  $Z$  exchange interaction and the combined effect of hyperfine interaction and NSI electron-nucleus  $Z$  exchange interaction.

The parameters describing nucleon-nucleon coupling, effect of NAM is subsumed into it, extracted from the Cs PNC experiment do not concur with the nuclear data [6]. This certainly calls for the further investigation of the NSD-PNC effects in other atomic systems as well. An example of an alternative experiment is the proposal to measure the PNC in  $\text{Ba}^+$  ion, suggested by Fortson [7] and is in progress at Seattle [8, 9]. This experiment could lead to an unambiguous observation of NAM in the  $6s^2S_{1/2} - 5d^2D_{5/2}$  transition, as the NSI-PNC alone does not contribute to this transition. It is important to note that the major difficulty to a clear observation of NAM is the large NSI signal, which overwhelms the NSD signature. The  $\text{Ra}^+$  ion has also been suggested and is considered to be an important candidate for the PNC measurement [10, 11]. Apart from  $\text{Ba}^+$  and  $\text{Ra}^+$  ions which are one-valence systems the other promising candidate for PNC, the NAM in particular, measurement is the atomic Yb. An enhanced effect of PNC has already been reported [12, 13] in neutral Yb, the  $6s^2^1S_0 - 6s5d^3D_2$  transition, and for further refinement of the experiment is in progress at Berkeley. The  $6s^2S_{1/2} - 5d^2D_{3/2}$  transition in  $\text{Yb}^+$ , has also been suggested to reveal the NAM signature and is being investigated at Los Alamos [14, 15].

The atomic theory results using reliable and accurate many-body methods are key to estimate the expected value of PNC transition amplitudes and extracting NAM. For the theoretical calculations, the relativistic coupled-cluster (RCC) theory [16, 17] can be of great significance, as it is one of the most reliable many-body theory to incorporate electron correlation in atomic calculations. The RCC has been used extensively in atomic structure calculations [10, 18–23] of properties like transition energies, hyperfine structure constants, electromagnetic transition amplitudes, intrinsic electric dipole moment and PNC in atoms. Apart from atomic physics, it has also been used with great success in nuclear [24], molecular [25] and the condensed matter [26] physics.

In this work, we employ perturbed relativistic coupled-cluster (PRCC) theory to calculate NSI and NSD-PNC amplitudes of the  $[4f^{14}]6s^2S_{1/2} - [4f^{14}]5d^2D_{3/2}$  transition in the case of  $^{171}\text{Yb}^+$  ion. This is timely as there are few theoretical results, Sahoo *et al* [27] and Dzuba *et al* [28] for NSI-PNC and Dzuba *et al* [28] and Porsev *et al* [29] for NSD-PNC are the previous works. The NSI-PNC results from Ref. [27] calculated using RCC method differ substantially from Ref. [28] where the correlation-potential-method with sum-over-state approach is employed to calculate NSI and NSD-PNC. The NSD-PNC results reported in Ref. [29] are based on RPA and, in general, is in agreement with the results reported in Ref. [28]. However, the later is based on the sum-over-state approach, at the level of PNC matrix elements. The PRCC method [30–32] employed in present work is different from the sum-over-states approach. It accounts for the all singly and doubly excited intermediate states. There are two sets of the cluster amplitudes in the PRCC, and the summation over states in the first order time-independent perturbation is incorporated in one set of the cluster amplitudes.

The paper is organized as follows. In Section. II, we provide a brief description of the theoretical methods. The unperturbed RCC equations for close-shell and one-valence systems are given to serve as a easy reference. The perturbed RCC is then discussed in detail and PRCC equations are derived. The expression for E1PNC using PRCC wave function and some leading order diagrams are also discussed. Results from the work and uncertainty

estimates are presented and discussed in Section. III.

## II. THEORETICAL METHODS

In absence of PNC interaction the atomic states are of definite parity, and we consider these as the eigen states of the no-virtual-pair Dirac-Coulomb Hamiltonian [33]

$$H^{\text{DC}} = \Lambda_+ \sum_{i=1}^N [c\boldsymbol{\alpha}_i \cdot \mathbf{p}_i + (\beta_i - 1)c^2 - V_N(r_i)] + \sum_{i<j} \frac{1}{r_{ij}} \Lambda_+, \quad (1)$$

where  $\boldsymbol{\alpha}_i$  and  $\beta$  are the Dirac matrices,  $\mathbf{p}$  is the linear momentum,  $V_N(r)$  is the nuclear Coulomb potential and the last term is the electron-electron Coulomb interactions. The operator  $\Lambda_+$  projects on the positive energy eigenstates to avoid the negative energy continuum solutions. The Hamiltonian  $H^{\text{DC}}$  satisfies the eigen value equation

$$H^{\text{DC}}|\Psi_v\rangle = E_v|\Psi_v\rangle, \quad (2)$$

where  $|\Psi_v\rangle$  is the exact atomic state of the one-valence system and  $E_v$  is the corresponding energy. Here after, for compact notation, we use  $H$  to represent  $H^{\text{DC}}$ . In the present work, we use RCC theory with the single and doubles (CCSD) excitation approximation to solve Eq. (2). In RCC,  $|\Psi_v\rangle$  is expressed in terms of the closed-shell and one-valence cluster operators,  $T^{(0)}$  and  $S^{(0)}$  respectively, as

$$|\Psi_v\rangle = e^{T^{(0)}} [1 + S^{(0)}] |\Phi_v\rangle, \quad (3)$$

where superscript (0) represents the unperturbed RCC operators. The one-valence Dirac-Fock (DF) reference state  $|\Phi_v\rangle$  is obtained by adding an electron to the closed-shell reference state,  $|\Phi_v\rangle = a_v^\dagger |\Phi_0\rangle$ . In the CCSD approximation,  $T^{(0)} = T_1^{(0)} + T_2^{(0)}$  and  $S^{(0)} = S_1^{(0)} + S_2^{(0)}$ . Using the second quantized representation

$$T_1 = \sum_{a,p} t_{ap}^p a_p^\dagger a_a, \text{ and } T_2 = \frac{1}{2!} \sum_{a,b,p,q} t_{ab}^{pq} a_p^\dagger a_q^\dagger a_b a_a, \quad (4a)$$

$$S_1 = \sum_p s_{vp}^p a_p^\dagger a_v, \text{ and } S_2 = \sum_{a,p,q} s_{va}^{pq} a_p^\dagger a_q^\dagger a_a a_v. \quad (4b)$$

Here,  $t_{\dots}$  and  $s_{\dots}$  are the cluster amplitudes. The indexes  $abc\dots$  ( $pqr\dots$ ) represent core (virtual) states and  $vwx\dots$  represent valence states. The operators  $T_1$  ( $S_1$ ) and  $T_2$  ( $S_2$ ) give single and double replacements after operating on the closed(open)-shell reference states. The diagrammatic representation of these operators are shown in Fig. 1.

The open-shell cluster operators are then the solutions of nonlinear equations [34]

$$\langle \Phi_v^p | \bar{H}_N + \{ \bar{H}_N S^{(0)} \} | \Phi_v \rangle = E_v^{\text{att}} \langle \Phi_v^p | S_1^{(0)} | \Phi_v \rangle, \quad (5a)$$

$$\langle \Phi_{va}^{pq} | \bar{H}_N + \{ \bar{H}_N S^{(0)} \} | \Phi_v \rangle = E_v^{\text{att}} \langle \Phi_{va}^{pq} | S_2^{(0)} | \Phi_v \rangle, \quad (5b)$$

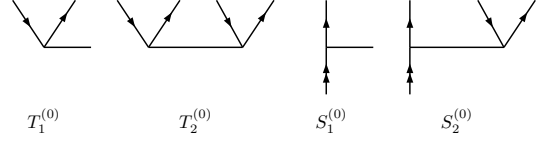


FIG. 1. Diagrammatic representation of the single and double excitation unperturbed cluster operators in closed shell and one-valence sectors.

where  $\bar{H}_N = e^{-T^{(0)}} H_N e^{T^{(0)}}$  is the similarity transformed Hamiltonian,  $H_N = H - \langle \Phi_0 | H | \Phi_0 \rangle$  is the normal ordered Hamiltonian and  $E_v^{\text{att}}$  is the attachment energy of the valence electron. The operators  $T^{(0)}$  are the solutions of a similar set of nonlinear coupled equations

$$\langle \Phi_a^p | \bar{H}_N | \Phi_0 \rangle = 0, \quad (6a)$$

$$\langle \Phi_{ab}^{pq} | \bar{H}_N | \Phi_0 \rangle = 0. \quad (6b)$$

The details on the derivation of these equations are given in our previous work [35].

In presence of PNC interaction atomic states mix with the opposite parity states and the total atomic Hamiltonian is

$$H_a = H^{\text{DC}} + \lambda H_{\text{PNC}}. \quad (7)$$

Here,  $\lambda$  is the perturbation parameter and  $H_{\text{PNC}}$  represents the any general PNC interaction Hamiltonian. It has two components, the NSI and NSD interaction. These are

$$H_{\text{PNC}}^{\text{NSI}} = \frac{G_F Q_W}{2\sqrt{2}} \sum_i \gamma_5 \rho_N(r_i), \quad (8a)$$

$$H_{\text{PNC}}^{\text{NSD}} = \frac{G_F \mu'_W}{\sqrt{2}I} \sum_i \boldsymbol{\alpha}_i \cdot \mathbf{I} \rho_N(r), \quad (8b)$$

where,  $G_F (= 2.22 \times 10^{-14} a.u.)$  is the Fermi coupling constant,  $Q_W$  and  $\mu'_W$  are respectively the weak nuclear charge and the weak nuclear moment of the nucleus expressed in terms of neutron and proton numbers,  $\boldsymbol{\alpha}$  and  $\gamma_5$  are the Dirac matrices,  $\rho_N(r)$  is the normalized nuclear density and  $I$  is the nuclear spin. Compared to the NSI-PNC, the NSD-PNC require two important considerations because of the nuclear spin operator  $\mathbf{I}$ . First, the cluster operators in the electron space are rank one operators, and second, the atomic states in the one-valence sector are eigenstates of total angular momentum  $\mathbf{F} = \mathbf{I} + \mathbf{J}$ .

Similar to the unperturbed eigen value equation, Eq. (2), we may write the perturbed eigenvalue equation, satisfied by the total atomic Hamiltonian, as

$$H_a |\tilde{\Psi}_v\rangle = \tilde{E}_v |\tilde{\Psi}_v\rangle, \quad (9)$$

where  $|\tilde{\Psi}_v\rangle$  is the perturbed atomic state and  $\tilde{E}_v$  is the corresponding energy. To the first-order in  $\lambda$ ,  $|\tilde{\Psi}_v\rangle = |\Psi_v\rangle + \lambda |\tilde{\Psi}_v^1\rangle$  and  $\tilde{E}_v = E_v + \lambda E_v^1$ , where the bar in  $|\tilde{\Psi}_v^1\rangle$  denotes it's parity is opposite to  $|\Psi_v\rangle$ . From here on, to

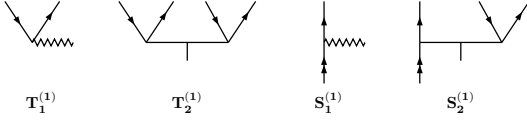


FIG. 2. Diagrammatic representation of the single and double excitation NSD-perturbed cluster operators in closed-shell and one-valence sectors. The extra line in the  $T_2^{(1)}$  and  $S_2^{(1)}$  is to indicate the multipole structure of the operators.

derive the PRCC equations we consider the NSD-PNC interaction Hamiltonian. Using Eq. (8b), we can rewrite Eq. (9) as

$$(H^{\text{DC}} + \lambda \mathbf{H}_{\text{elec}}^{\text{NSD}} \cdot \mathbf{I}) |\tilde{\Psi}_v\rangle = E_v |\tilde{\Psi}_v\rangle. \quad (10)$$

Here,  $H_{\text{elec}}^{\text{NSD}} = (G_F \mu'_W / \sqrt{2}) \sum_i \alpha_i \rho_N(r)$  is the electronic part of  $H_{\text{PNC}}^{\text{NSD}}$ . While writing above equation we have used  $E_v^1 = \langle \Psi_v | H_{\text{PNC}}^{\text{NSD}} | \Psi_v \rangle = 0$ , as  $H_{\text{PNC}}^{\text{NSD}}$  is an odd parity operator it connects opposite parity states only. In the PRCC theory, the perturbed wave function is expressed as

$$|\tilde{\Psi}_v\rangle = e^{T^{(0)}} [1 + \lambda \mathbf{T}^{(1)} \cdot \mathbf{I}] [1 + S^{(0)} + \lambda \mathbf{S}^{(1)} \cdot \mathbf{I}] |\Phi_v\rangle, \quad (11)$$

where  $\mathbf{T}^{(1)}$  and  $\mathbf{S}^{(1)}$  are the closed-shell and one-valence PRCC operators, respectively. The superscript (1) is used to indicate the perturbation. The diagrammatic

representation of these cluster operators are shown in Fig. 2.

Using Eq. (11) in Eq. (10), we can rewrite the eigenvalue equation as

$$\begin{aligned} (H + \lambda \mathbf{H}_{\text{elec}}^{\text{NSD}} \cdot \mathbf{I}) e^{T^{(0)}} [1 + \lambda \mathbf{T}^{(1)} \cdot \mathbf{I}] [1 + S^{(0)} \\ + \lambda \mathbf{S}^{(1)} \cdot \mathbf{I}] |\Phi_v\rangle = E_v e^{T^{(0)}} [1 + \lambda \mathbf{T}^{(1)} \cdot \mathbf{I}] [1 + S^{(0)} \\ + \lambda \mathbf{S}^{(1)} \cdot \mathbf{I}] |\Phi_v\rangle. \end{aligned} \quad (12)$$

To derive the PRCC equations, we project the above equation on  $e^{-T^{(0)}}$  and retain the terms linear in  $\lambda$ . In addition, for further simplification, we use normal-ordered form of the Hamiltonian  $H_N = H - \langle \Phi_v | H | \Phi_v \rangle$ . After these sequence of operations, the eigenvalue equation is modified to

$$\begin{aligned} [\bar{H}_N \mathbf{S}^{(1)} + \bar{H}_N \mathbf{T}^{(1)} (1 + S^{(0)}) + \bar{\mathbf{H}}_{\text{elec}}^{\text{NSD}} (1 + S^{(0)})] |\Phi_v\rangle \\ = [\Delta E_v \mathbf{S}^{(1)} + \Delta E_v \mathbf{T}^{(1)} (1 + S^{(0)})] |\Phi_v\rangle \end{aligned} \quad (13)$$

where  $\Delta E_v = E_v - \langle \Phi_v | H | \Phi_v \rangle$ , is the correlation energy of the one-valence system. Like  $\bar{H}_N$  introduced earlier,  $\bar{\mathbf{H}}_{\text{elec}}^{\text{NSD}} = e^{-T^{(0)}} H_{\text{elec}}^{\text{PNC}} e^{T^{(0)}}$  is the similarity transformed NSD-PNC interaction Hamiltonian in the electronic space. The PRCC equations of  $\mathbf{S}^{(1)}$  can now be derived by projecting Eq. (13) with the excited determinants  $\langle \Phi_v^p |$  and  $\langle \Phi_v^q |$  as

$$\langle \Phi_v^p | \{ \bar{H}_N \mathbf{S}^{(1)} \} + \{ \bar{H}_N \mathbf{T}^{(1)} \} + \{ \bar{H}_N \mathbf{T}^{(1)} S^{(0)} \} + \bar{\mathbf{H}}_{\text{elec}}^{\text{NSD}} + \{ \bar{\mathbf{H}}_{\text{elec}}^{\text{NSD}} S^{(0)} \} |\Phi_v\rangle = E_v^{\text{att}} \langle \Phi_v^p | \mathbf{S}_1^{(1)} |\Phi_v\rangle, \quad (14a)$$

$$\langle \Phi_v^q | \{ \bar{H}_N \mathbf{S}^{(1)} \} + \{ \bar{H}_N \mathbf{T}^{(1)} \} + \{ \bar{H}_N \mathbf{T}^{(1)} S^{(0)} \} + \bar{\mathbf{H}}_{\text{elec}}^{\text{NSD}} + \{ \bar{\mathbf{H}}_{\text{elec}}^{\text{NSD}} S^{(0)} \} |\Phi_v\rangle = E_v^{\text{att}} \langle \Phi_v^q | \mathbf{S}_2^{(1)} |\Phi_v\rangle. \quad (14b)$$

While deriving the equations we have used the relations  $\langle \Phi_v^p | \mathbf{T}^{(1)} |\Phi_v\rangle = 0$  and  $\langle \Phi_v^p | \mathbf{T}^{(1)} S |\Phi_v\rangle = 0$ . These follows as  $\mathbf{T}^{(1)}$  is an operator of closed-shell sector, it does not contribute to the PRCC equation of  $\mathbf{S}_1^{(1)}$  and  $\mathbf{S}_2^{(1)}$ . The closed-shell operators  $\mathbf{T}^{(1)}$  are the solutions of the similar set of coupled equations [35]

$$\langle \Phi_a^p | \{ \bar{H}_N \mathbf{T}^{(1)} \} |\Phi_0\rangle = -\langle \Phi_a^p | \bar{\mathbf{H}}_{\text{elec}}^{\text{NSD}} - \Delta E_0 \mathbf{T}^{(1)} |\Phi_0\rangle, \quad (15a)$$

$$\langle \Phi_{ab}^{pq} | \{ \bar{H}_N \mathbf{T}^{(1)} \} |\Phi_0\rangle = -\langle \Phi_{ab}^{pq} | \bar{\mathbf{H}}_{\text{elec}}^{\text{NSD}} - \Delta E_0 \mathbf{T}^{(1)} |\Phi_0\rangle, \quad (15b)$$

These equations can be derived from the closed-shell perturbed eigenvalue equation. We can also derive a similar set of PRCC equations for the NSI-PNC interaction Hamiltonian. One major difference is, the cluster operators are rank zero operators.

After solving the RCC and PRCC equations, we can use the atomic states for the properties calculations. The RCC expressions and the diagrams contributing to the hyperfine structure (HFS) constants and the E1 transi-

tion amplitudes are derived and discussed in our previous work [34]. In the present work, we use the same expressions and diagrams to compute HFS constants and E1 transition amplitudes. The PNC induced electric dipole transition amplitude, using PRCC wave function, is

$$\text{E1PNC} = \langle \tilde{\Psi}_w | \mathbf{D} | \tilde{\Psi}_v \rangle, \quad (16)$$

where  $\mathbf{D}$  is the dipole operator. This expression, unlike the conventional sum-over-states approach, implicitly account for all the possible intermediate states. From Eq. (11), for the NSD-PNC interaction, the transition amplitude is

$$\begin{aligned} E1_{\text{PNC}}^{\text{NSD}} = \langle \Phi_w | e^{T^{(0)\dagger}} [1 + \lambda \mathbf{T}^{(1)} \cdot \mathbf{I}]^\dagger [1 + S^{(0)} + \lambda \mathbf{S}^{(1)} \cdot \mathbf{I}]^\dagger \\ \mathbf{D} e^{T^{(0)}} [1 + \lambda \mathbf{T}^{(1)} \cdot \mathbf{I}] [1 + S^{(0)} + \lambda \mathbf{S}^{(1)} \cdot \mathbf{I}] |\Phi_v\rangle \end{aligned} \quad (17)$$

Consider terms linear in  $\lambda$  and retain only those up to second order in cluster amplitude. Define the electronic

component as  $E1_{\text{elec}}^{\text{NSD}}$ , corresponding to the  $H_{\text{elec}}^{\text{NSD}}$ , it is then given as

$$\begin{aligned}
E1_{\text{elec}}^{\text{NSD}} \approx & \langle \Phi_w \| \mathbf{DT}^{(1)} + T^{(0)\dagger} \mathbf{DT}^{(1)} + \mathbf{T}^{(1)\dagger} \mathbf{DT}^{(0)} \\
& + \mathbf{T}^{(1)\dagger} \mathbf{D} + \mathbf{DT}^{(1)} S^{(0)} + \mathbf{T}^{(1)\dagger} S^{(0)\dagger} \mathbf{D} \\
& + S^{(0)\dagger} \mathbf{DT}^{(1)} + \mathbf{T}^{(1)\dagger} \mathbf{DS}^{(0)} + \mathbf{DS}^{(1)} + \mathbf{S}^{(1)\dagger} \mathbf{D} \\
& + S^{(0)\dagger} \mathbf{DS}^{(1)} + \mathbf{S}^{(1)\dagger} \mathbf{DS}^{(0)} \| \Phi_v \rangle. \quad (18)
\end{aligned}$$

To calculate E1PNC, we use diagrammatic analysis to identify the Goldstone diagrams from these terms. However, we exclude the structural radiation diagrams, arising from the terms involving two-body cluster operators, for example,  $\mathbf{T}_2^{(1)} \mathbf{DT}_2^{(0)}$ . The selected diagrams from the leading order and next to leading order terms are shown in the Fig. 3.

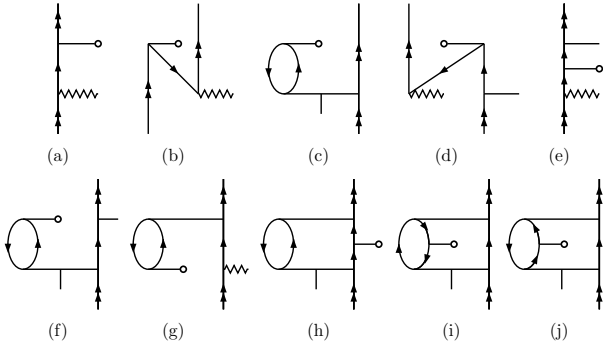


FIG. 3. Some of the leading order PRCC diagrams which contribute to the  $E1_{\text{elec}}^{\text{PNC}}$  of one-valence atoms.

### III. RESULTS AND DISCUSSIONS

#### A. Single-particle basis functions

For all the calculations we use Gaussian type orbitals (GTOs) or single particle wave functions with  $V^{N-2}$  potential. As mentioned earlier, to incorporate the relativistic effects we use the Dirac-Coulomb atomic Hamiltonian. For the nuclear potential we consider the finite size Fermi density distribution

$$\rho_{\text{nuc}}(r) = \frac{\rho_0}{1 + e^{(r-c)/a}}, \quad (19)$$

here,  $a = t4 \ln 3$ . The parameter  $c$  is the half-charge radius, that is  $\rho_{\text{nuc}}(c) = \rho_0/2$  and  $t$  is the skin thickness. The orbitals are of the form

$$\psi_{n\kappa m}(\mathbf{r}) = \frac{1}{r} \begin{pmatrix} P_{n\kappa}(r) \chi_{\kappa m}(\mathbf{r}/r) \\ iQ_{n\kappa}(r) \chi_{-\kappa m}(\mathbf{r}/r) \end{pmatrix}, \quad (20)$$

where  $P_{n\kappa}(r)$  and  $Q_{n\kappa}(r)$  are the large and small component radial wave functions,  $\kappa$  is the relativistic total angular momentum quantum number and  $\chi_{\kappa m}(\mathbf{r}/r)$  are

the spinor-spherical harmonics. The radial components are then defined as linear combination of Gaussian type functions [36, 37]

$$\begin{aligned}
P_{n\kappa}(r) &= \sum_p C_{\kappa p}^L g_{\kappa p}^L(r), \\
Q_{n\kappa}(r) &= \sum_p C_{\kappa p}^S g_{\kappa p}^S(r). \quad (21)
\end{aligned}$$

The index  $p = 1, 2, \dots, m$ , where  $m$  is the number of basis functions and  $C_{\kappa p}^{\dots}$  are the coefficients of linear combination. For large component we choose

$$g_{\kappa p}^L(r) = C_{m\kappa i}^L r^{n_\kappa} e^{-\alpha_p r^2}, \quad (22)$$

where  $n_\kappa$  is an integer and  $C_{m\kappa i}^L$  is the normalization constant. The small component are derived from the large components using kinetic balance condition. The  $\alpha_p$  follow the general relation

$$\alpha_p = \alpha_0 \beta^{p-1}. \quad (23)$$

The parameters,  $\alpha_0$  and  $\beta$ , are optimized such that the single particle energies of the core and valence orbitals are in good agreement with the numerical results, obtained from GRASP92 [38]. In Table. I, we compare the energy of the valence orbitals from the GTO with the GRASP92 data.

TABLE I. The valence orbital and SCF energies of Gaussian type orbitals (GTO) are compared with the GRASP92 data.

Orbitals	GTO	GRASP92
$6s^2 S_{1/2}$	-0.413668	-0.413665
$6p^2 P_{1/2}$	-0.301112	-0.301113
$6p^2 P_{3/2}$	-0.288305	-0.288307
$5d^2 D_{3/2}$	-0.303070	-0.303071
$5d^2 D_{5/2}$	-0.300885	-0.300886
$E_{\text{SCF}}$	-14067.0622	-14067.0676

#### B. Excitation energies, hyperfine structure constants and E1 transition amplitudes

The excitation energies, hyperfine structure constants and the E1 transition amplitudes from our calculations are listed in the Tables. II, III and IV, respectively. These results are obtained using a fairly large basis of 177 active GTOs, it consists of 19, 17, 17, 17, 15 and 13 orbitals in the  $s$ ,  $p$ ,  $d$ ,  $f$ ,  $g$  and  $h$  symmetries, respectively. To arrive at this basis set we start with a moderate size of 100 active orbitals with the combination  $12s$ ,  $10p$ ,  $10d$ ,  $10f$ ,  $8g$  and  $6h$ . And perform seven sets of calculations by adding one orbital to each symmetry in every successive sets. The % change in HFS constants and E1 transition amplitudes with respect to number of active orbitals are shown in Fig. 4. As we see in the

figure, the E1 transition amplitudes converge and there is no observable change in the amplitudes after 155. On the other hand, for HFS constants we observe a slower convergence pattern. It is evident from the figure that the HFS results are close to convergence. The maximum uncertainty is about 0.5%, in the case of  $5d^2D_{5/2}$ , but it is smaller for the states  $6s^2S_{1/2}$ ,  $6p^2P_{1/2}$ ,  $6p^2P_{3/2}$  and  $5d^2D_{3/2}$ , the uncertainties are 0.3%, 0.3%, 0.1% and 0.05%, respectively.

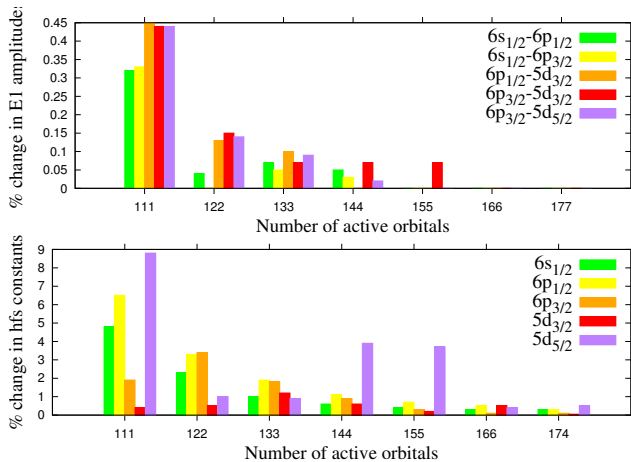


FIG. 4. The convergence (% change) of the hyperfine structure constants and the E1 transition amplitudes with respect to the number of active orbitals.

The excitation energies from our calculations are listed in Table. II. As described in Sec. II, these are calculated using RCC with the CCSD approximation. Except for the  $6p^2P_{3/2}$  excitation energy, our results are better or on par with the previous theoretical results when compared with the experimental data. The all-order results reported in Ref. [29] are closer to the experimental data than the other theoretical results, including the present work. For the  $6p^2P_{3/2}$ , our result is in close to the RCC result of Sahoo and collaborators [27]. Among the other three results for this level, our result is closer to the Ref. [29]. The dominant excitations which contribute to the denominator of the NSI-PNC matrix are  $6s^2S_{1/2} - 6p^2P_{1/2}$  and  $6p^2P_{1/2} - 5d^2D_{3/2}$ . However for the NSD-PNC, these are  $6s^2S_{1/2} - 6p^2P_{1/2}$ ,  $6p^2P_{1/2} - 5d^2D_{3/2}$ ,  $6s^2S_{1/2} - 6p^2P_{3/2}$  and  $6p^2P_{3/2} - 5d^2D_{3/2}$ . The accuracy achieved for these in the present work are 3.4%, 4.5%, 2.4% and 4.6%, respectively. We have incorporated these errors in the total uncertainty estimates for the PNC results.

In the Table. III we present, and compare HFS constants obtained from the present calculations with the other theoretical and experimental results. As evident from the table, our results for the  $6p^2P_{1/2}$ ,  $5d^2D_{3/2}$  and  $5d^2D_{5/2}$  states are in better agreement with the experimental data than the other theoretical results. However, for the  $6s^2S_{1/2}$  state, like the other theoretical

TABLE II. Excitation energy for some of the low lying excitations in  $^{171}\text{Yb}^+$ . The values are in  $\text{cm}^{-1}$ .

Level	This work	Other works	Exp.Ref[49].
$5d_{3/2}$	23983	23926 <sup>a</sup>	22961
		21238 <sup>b</sup>	
		22711 <sup>c</sup>	
		22820 <sup>d</sup>	
		22449 <sup>b</sup>	
$5d_{5/2}$	25576	24178 <sup>c</sup>	24333
		24261 <sup>d</sup>	
		28749 <sup>a</sup>	
		28048 <sup>b</sup>	
$6p_{1/2}$	27985	27945 <sup>c</sup>	27062
		27945 <sup>d</sup>	
		28109(1000) <sup>e</sup>	
		32376 <sup>a</sup>	
		31411 <sup>b</sup>	
$6p_{3/2}$	31757	31403 <sup>c</sup>	30392
		31481 <sup>d</sup>	
		31604(800) <sup>e</sup>	

<sup>a</sup> Reference[28].

<sup>b</sup> Reference[40].

<sup>c</sup> Reference[29]-MBPT + corrections.

<sup>d</sup> Reference[29]-All-order.

<sup>e</sup> Reference[27].

TABLE III. Magnetic dipole hyperfine structure constants of  $^{171}\text{Yb}^+$  in the unit MHz.

State	This work	Other works	Exp
$6s_{1/2}$	13488.314	13217 <sup>a</sup> , 13172 <sup>b</sup> ,	12645(2) <sup>e</sup>
		13091 <sup>c</sup> , 13332(1000) <sup>d</sup> ,	
$6p_{1/2}$	2348.036	12730(2) <sup>e</sup>	2104.9(1.3) <sup>e</sup>
		2533 <sup>a</sup> , 2350 <sup>b</sup> ,	
		2371 <sup>c</sup> , 2516(400) <sup>d</sup> ,	
$6p_{3/2}$	313.522	2317 <sup>e</sup>	877(20) <sup>f</sup>
		388 <sup>a</sup> , 311.5 <sup>b</sup> , 330 <sup>c</sup> ,	
		322(20) <sup>d</sup> , 391 <sup>e</sup>	
$5d_{3/2}$	421.131	291 <sup>a</sup> , 489 <sup>c</sup> , 447(20) <sup>d</sup> , 400.5 <sup>g</sup> ,	430(43) <sup>h</sup>
$5d_{5/2}$	-68.567	-96 <sup>c</sup> , -48(15) <sup>d</sup> , -12.6 <sup>g</sup>	-63.6(7) <sup>i</sup>

<sup>a</sup> Reference[28], <sup>b</sup> Reference[40], <sup>c</sup> Reference[29],

<sup>d</sup> Reference[27], <sup>e</sup> Reference[41], <sup>f</sup> Reference[43],

<sup>g</sup> Reference[42], <sup>h</sup> Reference[44], <sup>i</sup> Reference[45].

results, our result is also larger than the experimental result. Among the theoretical results, our result for this state is closer to the Ref. [27]. The reason for this is the method employed and the type of the orbitals used in the two works are similar. For the  $6p^2P_{3/2}$  state there is a large discrepancy between the theoretical results and experimental data. However, it must be emphasized that the experimental data is from a relatively old measurement. Our result lies between the third-order MBPT

results of Ref. [40] and the RCC result of Ref. [27].

The impact of the electron correlation effects is discernible in the Table. V, where we list the contributions from various RCC terms. The RCC terms in the table are based on the expression in our previous work [34]. The contribution listed as ‘‘Other’’ correspond to the terms  $S_2^\dagger H_{\text{hfs}} T + \text{c.c.}$  and  $S_2^\dagger H_{\text{hfs}} T S_1 + \text{c.c.}$ . As expected, the dominant contribution is from the DF term. It contributes approximately about 72%, 66%, 58%, 69% and 110% for the states  $6s^2 S_{1/2}$ ,  $6p^2 P_{1/2}$ ,  $6p^2 P_{3/2}$ ,  $5d^2 D_{3/2}$  and  $5d^2 D_{5/2}$ , respectively. Our DF value 9716.7 and 1548.2 for states  $6s^2 S_{1/2}$  and  $6p^2 P_{1/2}$ , respectively are on the higher side of the values, 9577 and 1542, reported by Safronova and collaborators in their recent work [29]. On the other hand, for the  $6p^2 P_{3/2}$ ,  $5d^2 D_{3/2}$  and  $5d^2 D_{5/2}$  states our results of 182.5, 289.7 and 110.2, show a close match with the values 183, 290 and 111 from Ref. [29]. The next two leading order contributions are from the terms  $S_1^\dagger \tilde{H}_{\text{hfs}} + \text{c.c.}$  and  $S_2^\dagger \tilde{H}_{\text{hfs}} + \text{c.c.}$ . Unlike other states,  $5d^2 D_{5/2}$  shows a different correlation pattern and contribution from  $S_2^\dagger \tilde{H}_{\text{hfs}} + \text{c.c.}$  is about -321% of the total value. However  $S_1^\dagger \tilde{H}_{\text{hfs}} + \text{c.c.}$  contributes 44% of the total value. Despite the large cancellations our total result compares well with the experiment.

TABLE IV. The electric dipole transition amplitudes of  $^{171}\text{Yb}^+$ .

Transition	This work	Other works	Exp.
$6p_{1/2} \leftarrow 6s_{1/2}$	2.748	2.72 <sup>a</sup> , 2.73 <sup>b</sup> , 2.75 <sup>c</sup> , 2.64 <sup>d</sup> , 2.72(1) <sup>e</sup>	2.47(3) <sup>f</sup>
$6p_{3/2} \leftarrow 6s_{1/2}$	3.901	3.84 <sup>a</sup> , 3.84 <sup>b</sup> , 3.83 <sup>c</sup> , 3.71 <sup>d</sup> , 3.83(1) <sup>e</sup>	3.36(3) <sup>g</sup>
$5d_{3/2} \leftarrow 6p_{1/2}$	3.138	3.09 <sup>a</sup> , 3.78 <sup>b</sup> , 3.06 <sup>c</sup> , 2.98 <sup>d</sup> , 3.06(2) <sup>e</sup>	2.97(4) <sup>f</sup>
$5d_{3/2} \leftarrow 6p_{3/2}$	1.369	1.36 <sup>a</sup> , 1.55 <sup>b</sup> , 1.35 <sup>c</sup> , 1.32 <sup>d</sup> , 1.35(2) <sup>e</sup>	–
$5d_{5/2} \leftarrow 6p_{3/2}$	4.307	4.77 <sup>b</sup> , 4.23 <sup>c</sup> , 4.23(3) <sup>e</sup>	–

<sup>a</sup> Reference[28].

<sup>b</sup> Reference[40].

<sup>c</sup> Reference[29]- MBPT + corrections.

<sup>d</sup> Reference[29]- All-order.

<sup>e</sup> Reference[27].

<sup>f</sup> Reference[46, 47].

<sup>g</sup> Reference[48].

The E1 transition amplitudes are presented in the Table. IV. For comparison the results from the other theoretical and experimental works are also listed. Like HFS constant, transition amplitudes are calculated using the RCC wave functions. We have used the similar expressions and diagrams as the HFS except for one key difference, the hyperfine operator is replaced by the dipole operator. The experimental results are available only for the  $6s^2 S_{1/2} - 6p^2 P_{1/2}$ ,  $6s^2 S_{1/2} - 6p^2 P_{3/2}$  and

$6p^2 P_{1/2} - 5d^2 D_{3/2}$  transitions. Among all the theoretical results, the results from the recent all-order work [29] are closest to the experimental data. All other results, including ours, are on the higher side of the experimental value. The component wise contributions are listed in the Table. V. Like in the case of HFS constant, the DF term has the dominant contribution. It contributes approximately about 118%, 116%, 123%, 124% and 121%, respectively, for the transitions listed in the table. A close agreement is observed in the DF data from our calculation with the Ref. [29].

### C. NSI-E1PNC

For calculation of NSI-E1PNC, we use the expression Eq. (18) derived for NSD-E1PNC in the electronic space. However, the important difference in this case is, as mentioned earlier, the PRCC cluster operators are rank zero operators. In terms of diagrams, the ones with dominant contributions are derived from Fig. 3 with the NSD-perturbed operators replaced by the NSI-perturbed ones. In Table. VI, we list the contributions from the different terms in PRCC. Among all the terms, the largest contribution, about 117% of the total value, is from  $DS_1^{(1)}$ . The reason for this, as evident from Table. VII, is the large  $H_{\text{PNC}}$  mixing between  $6s^2 S_{1/2}$  and  $np^2 P_{1/2}$  orbitals. This large contribution from  $DS_1^{(1)}$  is consistent with the pattern of correlation reported in Ref. [27]. The next leading order contributions are  $DS_2^{(1)} + \text{H.c.}$  and  $T_1^{(1)\dagger} D$ . The former involve one core and one virtual orbitals, and the later connects  $T_1^{(1)\dagger}$  and  $D$  through a core orbital. These contribute about -17% and 15%, respectively. The terms  $S_2^{(0)\dagger} DS_1^{(0)} + \text{H.c.}$  and  $S_1^{(0)\dagger} DS_1^{(0)} + \text{c.c.}$  are third and fourth leading order terms, contributing about -7% each. The contribution from normalization is -2.8%. Small but not insignificant contributions of 2% and -1.8% are also observed from the terms  $T_2^{(0)\dagger} DT_1^{(1)} + \text{c.c.}$  and  $S_1^{(1)\dagger} D$ , respectively.

To examine the correlation pattern more closely we pick the leading order terms  $DS_1^{(1)}$  and  $T_1^{(1)\dagger} D$ , and for these we calculate the E1PNC contributions from various intermediate  $np_{1/2}$  states. The dominant contributions from these are tabulated in Table. VII. The same analysis but at the DF level is presented in Table. VIII. As we see in both the tables, dominant contribution is from the  $6p^2 P_{1/2}$  state, contributing about 117% of the total value. The reason for this is, large  $H_{\text{PNC}}$  induced mixing with the energetically closer  $6s^2 S_{1/2}$  state. The PRCC value is about 42% larger than the Dirac-Fock contribution. This can be attributed to the large amplitude of  $S_1^{(1)}$ , and hence to the correlation effects incorporated using PRCC. The next dominant contribution among the core orbital is  $5p_{1/2}$ . This contributes to  $T_1^{(1)\dagger} D$  through

TABLE V. Magnetic dipole hyperfine constants and E1 transition amplitudes, contributions from different terms in the RCC. The operator “O” here represents the hyperfine interaction Hamiltonian  $H_{\text{hfs}}$  for HFS constant and the dipole operator  $D$  for the E1 transition amplitudes.

State/Transition	Coupled-cluster terms								
	DF	$\tilde{O}$ - DF	$S_1^\dagger \tilde{O}$ +c.c.	$S_2^\dagger \tilde{O}$ +c.c.	$S_2^\dagger \tilde{O} S_1$ +c.c.	$S_1^\dagger \tilde{O} S_1$	$S_2^\dagger \tilde{O} S_2$	Other	Norm
$6s_{1/2}$	9716.682	-427.318	2756.071	1145.559	125.344	204.287	243.111	-49.371	-225.956
$6p_{1/2}$	1548.208	-49.951	528.950	245.862	28.191	46.824	23.105	22.266	-45.402
$6p_{3/2}$	182.531	-5.430	56.715	53.520	5.802	4.570	18.932	1.897	-5.012
$5d_{3/2}$	289.667	7.017	82.212	4.875	3.863	5.924	30.457	4.316	-7.197
$5d_{5/2}$	110.234	4.187	29.781	-220.089	-16.443	2.032	19.468	1.186	1.076
$6p_{1/2} \leftarrow 6s_{1/2}$	3.242	0.001	-0.175	-0.311	-0.010	0.019	0.029	0.006	-0.052
$6p_{3/2} \leftarrow 6s_{1/2}$	4.543	0.004	-0.254	-0.378	-0.012	0.023	0.037	0.006	-0.067
$5d_{3/2} \leftarrow 6p_{1/2}$	3.861	0.005	-0.437	-0.287	-0.003	0.032	0.034	-0.004	-0.068
$5d_{3/2} \leftarrow 6p_{3/2}$	1.697	0.002	-0.206	-0.121	-0.000	0.012	0.013	-0.001	-0.027
$5d_{5/2} \leftarrow 6p_{3/2}$	5.200	0.010	-0.566	-0.326	-0.001	0.034	0.036	0.005	-0.079

the  $H_{\text{PNC}}$  perturbed  $6s \ ^2S_{1/2}$ . In this case as well PRCC contribution is larger than the DF.

The total NSI-E1PNC result from our calculation is presented in Table. X. We have also listed the DF contribution. The other two theoretical results are based on the calculations with correlation-potential-method [28] and RCCSD(T) [27]. The E1PNC result from these two works differ from each other substantially. The CCSD(T) result from Ref. [27] is about 26% larger than Ref. [28]. Our DF value is marginally on the higher side of the value reported in Ref. [27]. However, the total result lies between Refs. [28] and [27], but closer to the coupled-cluster result of Ref. [27].

#### D. NSD-E1PNC

For the NSD-PNC, the dominant contributions from various PRCC terms in Eq. (18) are listed in Table. VI. For hyperfine transitions  $F_v = 0 \rightarrow F_w = 1$  and  $F_v = 1 \rightarrow F_w = 2$ , like in NSI-PNC,  $DS_1^{(1)}$  is the leading order term. It contributes about 231% and -130%, respectively. For transition  $F_v = 1 \rightarrow F_w = 1$ , however,  $S^{(1)\dagger}D$  is the dominant term, contributing about -123% of the total value. The same trend is reported in Ref. [28], where the contributions are about 252%, -226% and -157%, respectively, for the  $F_v = 0 \rightarrow F_w = 1$ ,  $F_v = 1 \rightarrow F_w = 1$  and  $F_v = 1 \rightarrow F_w = 2$  transitions. The next leading order term,  $S^{(1)\dagger}D$ , contribute about -114% and 35%, respectively to the  $F_v = 0 \rightarrow F_w = 1$  and  $F_v = 1 \rightarrow F_w = 2$  transitions. However, the second leading order term is  $DS_1^{(1)}$  for the  $F_v = 1 \rightarrow F_w = 1$  transition, it contributes about 69%. The next two leading order terms are  $T^{(1)\dagger}D$  and  $DS_2^{(1)} + \text{H.c.}$ . The contributions from these terms, in the sequence listed in Table. VI, are 39%, 11% and -22%, and -24%, -59% and -4%, re-

spectively. Non-negligible contributions are also observed from the terms  $T_2^{(0)\dagger}DT_1^{(0)} + \text{c.c.}$ ,  $S_1^{(0)\dagger}DS_1^{(0)} + \text{c.c.}$  and  $S_2^{(0)\dagger}DS_1^{(0)} + \text{c.c.}$

Unlike NSI-PNC, in NSD-PNC  $np_{3/2}$  states also contribute to the E1PNC matrix element. In Table. IX, we list dominant contributions from odd parity  $np_{1/2}$  and  $np_{3/2}$  states in the PRCC calculations for the  $F_v = 0 \rightarrow F_w = 1$  transition, and specifically the contributions from  $DS_1^{(1)}$ ,  $S^{(1)\dagger}D$  and  $T^{(1)\dagger}D$ . At DF level we present the contributions from the  $np_{1/2}$  states in Table. VIII. As we see in these tables, both at DF and PRCC levels, the dominant contribution is from the  $6p \ ^2P_{1/2}$  state. The total contribution from this in the PRCC calculations is about 150%, which can be attributed to the 230% and -79% contributions from  $DS_1^{(1)}$  and  $S^{(1)\dagger}D$ , respectively. The large contribution through  $DS_1^{(1)}$  is due to the strong  $H_{\text{PNC}}$  mixing with  $6s \ ^2S_{1/2}$ . However that is not the case with  $5d \ ^2D_{3/2}$ , which contributes through  $S^{(1)\dagger}D$ . At DF level  $6p \ ^2P_{1/2}$  contributes only through mixing with  $6s \ ^2S_{1/2}$ , and contribution is about 214%. The state  $6p \ ^2P_{3/2}$  is the third most dominant contributing one, contributing about -40%, through  $H_{\text{PNC}}$  perturbed  $5d \ ^2D_{3/2}$ . The other higher energy orbitals have negligible contribution.

The NSD-E1PNC total results are given in Table. X. For comparison we have listed the DF contributions. Our DF results 6.915, 1.632 and -3.643 for the three hyperfine transitions listed in Table. X compare well with the results 6.90, 1.70 and -3.70, reported in Ref. [29]. Our total results, however, are on the higher side of the random-phase approximation (RPA) based results from Ref. [29] for all hyperfine transitions. The other theoretical NSD-PNC data available for comparison is from Dzuba et al [28] using the correlation-potential-method. Our results for transitions  $F_v = 0 \rightarrow F_w = 1$  and

TABLE VI. The NSI and NSD E1PNC component wise contribution from various terms in the PRCC. The NSI and NSD contributions are listed in the units of  $iea_0 \times 10^{-11}(-Q_W/N)$  and  $iea_0\mu_W \times 10^{-12}$ , respectively.

Transition	$DS_1^{(1)}$	$S^{(1)\dagger}_1 D$	$DT_1^{(1)}$	$T^{(1)\dagger}_1 D$	$DS_2^{(1)}$	$T^{(0)\dagger}_1 DT_1^{(1)}$	$T^{(0)\dagger}_2 DT_1^{(1)}$	$S^{(0)\dagger}_1 DS_1^{(1)}$	$S^{(0)\dagger}_2 DS_1^{(1)}$	$T^{(1)\dagger}_1 DS_2^{(0)}$	Other	Norm	
					+c.c.	+c.c.	+c.c.	+c.c.	+c.c.	+c.c.			
NSI-PNC													
	8.950	-0.139	-0.005	1.179	-1.278	-0.025	0.168	-0.511	-0.529	0.028	0.003	-0.215	
NSD-PNC													
$F_w$	$F_v$												
1	0	6.689	-3.301	0.030	1.118	-0.683	0.001	-0.250	-0.239	-0.279	-0.008	-0.099	-0.083
1	1	1.431	-2.539	-0.002	0.221	-1.221	0.000	-0.061	0.026	0.038	0.008	-0.021	0.059
2	1	-3.590	0.952	-0.020	-0.608	-0.114	0.000	0.130	0.163	0.194	0.009	0.053	0.079

TABLE VII. The NSI E1PNC dominant contribution from the intermediate odd parity states in the PRCC. The listed E1PNC values are in the units of  $iea_0 \times 10^{-11}(-Q_W/N)$ .

$DS_1^{(1)}$				$T^{(1)\dagger}_1 D$			
D	$S_1^{(1)}$	E1PNC	state	D	$T^{(1)\dagger}_1$	E1PNC	state
-3.861	100.787	8.918	$6p_{1/2}$	0.003	-1.184	0.0	$2p_{1/2}$
-0.217	-29.596	-0.147	$7p_{1/2}$	-0.010	2.753	-0.001	$3p_{1/2}$
0.047	16.932	-0.018	$8p_{1/2}$	-0.008	7.623	-0.002	$4p_{1/2}$
-0.009	-21.986	-0.005	$9p_{1/2}$	1.290	39.984	1.182	$5p_{1/2}$
0.106	-29.329	0.071	$10p_{1/2}$				
-0.161	23.995	0.088	$11p_{1/2}$				
-0.096	15.017	0.033	$12p_{1/2}$				

$F_v = 1 \rightarrow F_w = 2$  are in good agreement with their results. For transition  $F_v = 1 \rightarrow F_w = 1$ , however, our result is higher than their value.

### E. Uncertainty estimates

To calculate the uncertainty of our E1PNC results we resort to a analysis based on the sum-over-state approach. In this method, the net uncertainty associated with an intermediate state is

$$\Delta = \delta E^{\text{exci}} + \delta E1 + \delta H_{\text{PNC}}, \quad (24)$$

where  $\delta E^{\text{exci}}$  and  $\delta E1$  are the deviations of excitation energy and E1 matrix element from the experimental data. And these are calculated based on results presented in Tables. II and IV, respectively. For  $\delta H_{\text{PNC}}$ , uncertainty associated with  $H_{\text{PNC}}$  matrix, we resort to the deviation of  $\sqrt{A_i A_f}$  from experimental data, where  $A_i$  and  $A_f$  represent the magnetic dipole hyperfine constants of initial and final states of the E1PNC transition.

As discussed earlier, dominant contribution to NSI-PNC is from the  $6p \ ^2P_{1/2}$  state, which contributes through  $DS_1^{(1)}$  i.e.  $H_{\text{PNC}}$  matrix element  $\langle 6p \ ^2P_{1/2} | H_{\text{PNC}} | 6s \ ^2S_{1/2} \rangle$ ,  $E1$  matrix  $\langle 5d \ ^2D_{3/2} | D | 6p \ ^2P_{1/2} \rangle$  and energy denominator

$E_{6s_{1/2}} - E_{6p_{1/2}}$ . The uncertainty associated with  $H_{\text{PNC}}$  matrix element, we get using our RCC results for hyperfine constants, is 9.1%. And, the relative uncertainty of  $E1$  matrix element and the energy denominator are calculated as 5.7% and 3.4%, respectively. Combining these, the net uncertainty in NSI-PNC result is 18.2%.

For NSD-PNC as well  $6p \ ^2P_{1/2}$  is the dominant contributing state. However in this case unlike NSI-PNC, apart from  $DS_1^{(1)}$ , contribution through  $S^{(1)\dagger}_1 D$  is not negligible. The matrix elements involve in this case are  $\langle 5d \ ^2D_{3/2} | H_{\text{PNC}} | 6p \ ^2P_{1/2} \rangle$  and  $\langle 6p \ ^2P_{1/2} | D | 6s \ ^2S_{1/2} \rangle$ , and the energy denominator is  $E_{6p_{1/2}} - E_{5d_{3/2}}$ . Using the similar analysis we get 4.52%, 11.26% and 2.41%, respectively for  $\delta H_{\text{PNC}}$ ,  $\delta E1$  and  $\delta E$ . Combining these, we get 18.19% as the net uncertainty associated with term  $S^{(1)\dagger}_1 D$ . The *rms* relative uncertainty in NSD-PNC results are then 18.17%.

## IV. CONCLUSIONS

In this work, we present NSI and NSD-PNC transition amplitudes for the  $[4f^{14}]6s^2 \ S_{1/2} - [4f^{14}]5d^2 \ D_{3/2}$  transition in  $^{171}\text{Yb}^+$  ion. To estimate the uncertainty of the the PNC results, we also calculate excitation energies, hyperfine structure constants and E1 transition amplitudes for some of the important low lying states, using RCC theory. The E1PNC results are computed using PRCC theory, which is formulated based on RCC theory and it incorporates electron correlation effects arising from a class of diagrams to all order in the presence of PNC interaction as a perturbation.

Our results for excitation energies, hyperfine structure constants and E1 transition amplitudes are in good agreement, in some cases better, with the previous experimental data. Our NSI-PNC result lies between the results from two previous studies reported in Refs. [28] and [27]. The NSD-PNC DF results from our work is in excellent agreement with the results reported in Ref. [29] for all hyperfine transitions. The total NSD-PNC result for the  $F_v = 0 \rightarrow F_w = 1$  hyperfine transition lies between the results of Refs. [28] and [29]. For the remaining two, our



TABLE VIII. The Dirac-Fock dominant contributions from the intermediate odd parity states. The listed NSI-E1PNC and NSD-E1PNC values are in the units of  $iea_0 \times 10^{-11}(-Q_W/N)$  and  $iea_0 \times 10^{-12}\mu'_W$ , respectively.

$DH_{\text{PNC}}$				$H_{\text{PNC}}D$			
D	$H_{\text{PNC}}$	E1PNC	state	D	$H_{\text{PNC}}$	E1PNC	state
NSI-PNC							
-3.861	71.073	6.288	$6p_{1/2}$	0.003	-1.178	0.0	$2p_{1/2}$
-0.217	-18.657	-0.092	$7p_{1/2}$	-0.010	2.657	-0.001	$3p_{1/2}$
0.047	10.547	-0.011	$8p_{1/2}$	-0.008	6.738	-0.001	$4p_{1/2}$
-0.009	-13.620	-0.003	$9p_{1/2}$	1.290	23.438	0.693	$5p_{1/2}$
NSD-PNC							
-3.861	-118.154	6.210	$6p_{1/2}$	0.003	1.957	0.0	$2p_{1/2}$
-0.217	31.016	-0.092	$7p_{1/2}$	-0.010	-4.417	-0.001	$3p_{1/2}$
0.047	-17.534	-0.011	$8p_{1/2}$	-0.008	-11.202	-0.001	$4p_{1/2}$
-0.009	22.642	-0.003	$9p_{1/2}$	1.290	-38.965	0.684	$5p_{1/2}$

TABLE IX. The NSD E1PNC dominant contribution from the intermediate odd parity states in the PRCC. The E1PNC values are in the units of  $iea_0 \times 10^{-12}\mu'_W$ . The contributions listed from the core  $nP_{1/2}$  and  $nP_{3/2}$  orbitals are from the terms  $T^{(1)\dagger}_1 D$  and  $DT^{(1)}$ , respectively.

$DS^{(1)}_1$			$S^{(1)\dagger}_1 D$			Orbital	$T^{(1)\dagger}_1 D / DT^{(1)}$			Orbital
D	$S^{(1)}_1$	E1PNC	D	$S^{(1)\dagger}_1$	E1PNC		D	$T^{(1)\dagger}_1$	E1PNC	
-3.861	-126.570	6.653	3.242	78.106	-2.298	$6p_{1/2}$	0.003	1.965	0.000	$2p_{1/2}$
-0.217	37.839	-0.112	-0.93	-9.111	-0.008	$7p_{1/2}$	-0.010	-4.550	-0.001	$3p_{1/2}$
0.047	-21.776	-0.013	0.011	4.704	-0.001	$8p_{1/2}$	-0.008	-12.416	-0.001	$4p_{1/2}$
-0.009	28.408	-0.004	0.013	-5.743	0.001	$9p_{1/2}$	1.290	-63.798	1.120	$5p_{1/2}$
0.106	38.534	0.056	0.075	-6.647	0.005	$10p_{1/2}$				
-0.161	-32.883	0.072	-0.081	4.431	0.003	$11p_{1/2}$				
-0.096	-22.179	0.029	-0.053	1.876	0.001	$12p_{1/2}$				
1.697	-8.244	0.000	-4.543	30.184	-0.984	$6p_{3/2}$	-0.001	-0.001	0.000	$2p_{3/2}$
0.024	2.418	0.000	0.358	-5.101	-0.013	$7p_{3/2}$	0.006	0.002	0.000	$3p_{3/2}$
0.008	-1.376	0.000	-0.140	2.786	-0.003	$8p_{3/2}$	0.046	0.109	0.000	$4p_{3/2}$
-0.028	1.845	0.000	0.136	-3.670	-0.004	$9p_{3/2}$	0.749	-3.964	0.021	$5p_{3/2}$
0.075	-2.226	0.000	-0.050	4.445	-0.002	$10p_{3/2}$				
0.080	-1.527	0.000	0.022	3.370	0.001	$11p_{3/2}$				
0.043	-0.791	0.000	0.035	1.675	0.000	$12p_{3/2}$				

TABLE X. The total NSI (in the unit  $iea_0 \times 10^{-11}(-Q_W/N)$ ) and NSD (in the unit  $iea_0\mu'_W \times 10^{-12}$ ) E1PNC results compared with the previous theoretical results.

Transition	This work		Other works
	DF	PRCC	
NSI-PNC			
$\langle 5d_{3/2}   \leftarrow \langle 6s_{1/2}  $	7.002	7.626	6.262(20) <sup>a</sup> , 8.470 <sup>b</sup>
NSD-PNC			
$\langle 5d_{3/2}, F_w = 1   \leftarrow \langle 6s_{1/2}, F_v = 0  $	6.915	2.896	3.1(1.9) <sup>a</sup> , 2.6 <sup>c</sup>
$\langle 5d_{3/2}, F_w = 1   \leftarrow \langle 6s_{1/2}, F_v = 1  $	1.632	-2.061	-1.3(4) <sup>a</sup> , -1.5 <sup>c</sup>
$\langle 5d_{3/2}, F_w = 2   \leftarrow \langle 6s_{1/2}, F_v = 1  $	-3.643	-2.753	-2.6(1.3) <sup>a</sup> , -2.2 <sup>c</sup>

<sup>a</sup> Reference[28]. <sup>b</sup> Reference[27]. <sup>c</sup> Reference[29].

results are slightly on the higher side. The upper bound to the theoretical uncertainty associated with E1PNC results is about 20%.

## ACKNOWLEDGMENTS

The author wish thank S. Chattopadhyay for useful discussions. The results presented in the paper are based on computations using the HPC cluster at Physical Research Laboratory, Ahmedabad.

- 
- [1] I. B. Khriplovich, *Parity Nonconservation in Atomic Phenomena* (Gordon and Breach, New York, 1991).
- [2] C. S. Wood *et al.*, *Science* **275**, 1759 (1997).
- [3] V. V. Flambaum and I. B. Khriplovich, *Zh. Exp. Teor. Fiz* **79**, 1656 (1980) [*Sov. Phys. JETP* **52** 835 (1980)].
- [4] V. V. Flambaum, I. B. Khriplovich, and O. P. Sushkov, *Phys. Lett. B* **146**, 367 (1984).
- [5] Y. Zel'dovich, *JETP* **6**, 1184 (1958).
- [6] W. C. Haxton and C. E. Wieman, *Annu. Rev. Nucl. Part. Sci.* **51**, 261 (2001).
- [7] N. Fortson, *Phys. Rev. Lett.* **70**, 2383 (1993).
- [8] J. A. Sherman, T. W. Koerber, A. Markhotok, W. Nagourney, and E. N. Fortson, *Phys. Rev. Lett.* **94**, 243001 (2005).
- [9] J. A. Sherman, A. Andalkar, W. Nagourney, and E. N. Fortson, *Phys. Rev. A* **78**, 052514 (2008).
- [10] L. W. Wansbeek *et al.*, *Phys. Rev. A* **78**, 050501(R) (2008).
- [11] O. O. Versolato *et al.*, *Phys. Rev. A* **82**, 010501(R) (2010).
- [12] K. Tsigutkin, *et al.*, *Phys. Rev. Lett.* **103**, 071601 (2009).
- [13] K. Tsigutkin, *et al.*, *Phys. Rev. A* **81**, 032114 (2010).
- [14] B. P. Das, *Proceedings of the Workshop on Violations of Fundamental Symmetries in Atoms and Nuclei, INT, Seattle, 1999* (unpublished).
- [15] J. Torgerson, private communication (2010).
- [16] F. Coester, *Nucl. Phys.* **7**, 421 (1958).
- [17] F. Coester and H. Kümmel, *Nucl. Phys.* **17**, 477 (1960).
- [18] E. Eliav, U. Kaldor, and Y. Ishikawa, *Phys. Rev. A* **53**, 3050 (1996).
- [19] R. Pal, *et al.*, *Phys. Rev. A* **75**, 042515 (2007).
- [20] B. K. Sahoo, L. W. Wansbeek, K. Jungmann, and R. G. E. Timmermans, *Phys. Rev. A* **79**, 052512 (2009).
- [21] H. S. Nataraj, B. K. Sahoo, B. P. Das, and D. Mukherjee, *Phys. Rev. Lett.* **101**, 033002 (2008).
- [22] R. Pal, D. Jiang, M. S. Safronova, and U. I. Safronova, *Phys. Rev. A* **79**, 062505 (2009).
- [23] S. G. Porsev, K. Beloy, and A. Derevianko, *Phys. Rev. D* **82**, 036008 (2010).
- [24] G. Hagen, T. Papenbrock, D. J. Dean, and M. Hjorth-Jensen, *Phys. Rev. Lett.* **101**, 092502 (2008).
- [25] T. A. Isaev, *et al.*, *Phys. Rev. A* **69**, 030501(R) (2004).
- [26] R. F. Bishop, P. H. Y. Li, D. J. J. Farnell, and C. E. Campbell, *Phys. Rev. B* **79**, 174405 (2009).
- [27] B. K. Sahoo and B. P. Das, *Phys. Rev. A* **84**, 010502(R) (2011).
- [28] V. A. Dzuba and V. V. Flambaum, *Phys. Rev. A* **83**, 052513 (2011).
- [29] S. G. Porsev, M. S. Safronova, and M. G. Kozlov *Phys. Rev. A* **86**, 022504 (2012).
- [30] S. Chattopadhyay, B. K. Mani, and D. Angom *Phys. Rev. A* **86**, 022522 (2012).
- [31] K. V. P. Latha, D. Angom, B. P. Das, and D. Mukherjee, *Phys. Rev. Lett.* **103**, 083001 (2009).
- [32] B. K. Mani and D. Angom, arXiv:1104.3473v1.
- [33] J. Sucher, *Phys. Rev. A* **22**, 348 (1980).
- [34] B. K. Mani and D. Angom, *Phys. Rev. A* **81**, 042514 (2010).
- [35] B. K. Mani, K. V. P. Latha, and D. Angom, *Phys. Rev. A* **80**, 062505 (2009).
- [36] A. K. Mohanty and E. Clementi, *Chem. Phys. Lett.*, **157**, 348 (1989).
- [37] R. K. Chaudhuri, P. K. Panda, and B. P. Das, *Phys. Rev. A* **59**, 1187 (1999).
- [38] F. A. Parpia, C. Froese Fischer, and I. P. Grant, *Comp. Phys. Comm.* **94**, 249 (1996).
- [39] P. Pulay, *Chem. Phys. Lett.* **73**, 393 (1980).
- [40] U. I. Safronova and M. S. Safronova, *Phys. Rev. A* **79**, 022512 (2009).
- [41] A. M. Martensson-Pendrill, D. S. Gough, and P. Hannaford, *Phys. Rev. A* **49**, 3351 (1994).
- [42] W. M. Itano, *Phys. Rev. A* **73**, 022510 (2006).
- [43] R. W. Berends and L. Maleki, *J. Opt. Soc. Am. B* **9**, 332 (1992).
- [44] D. Engelke and C. Tamm, *Europhys. Lett.* **33**, 347 (1996).
- [45] M. Roberts *et al.*, *Phys. Rev. A* **60**, 2867 (1999).
- [46] S. Olmschenk *et al.*, *Phys. Rev. A* **76**, 052314 (2007).
- [47] S. Olmschenk *et al.*, *Phys. Rev. A* **80**, 022502 (2009).
- [48] E. H. Pinnington, G. Rieger, and J. A. Kernahan, *Phys. Rev. A* **56**, 2421 (1997).
- [49] *NIST Atomic Spectroscopic Database*, <http://physics.nist.gov/PhysRefData>.
- [50] V. A. Dzuba, V. V. Flambaum, P. G. Silvestrov, and O. P. Sushkov, *J. Phys. B* **20**, 1399 (1987).